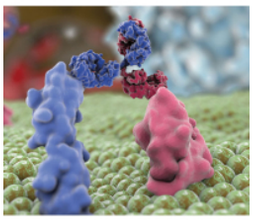

mAbs

ISSN: (Print) (Online) Journal homepage: https://www.tandfonline.com/loi/kmab20

Improved antibody pharmacokinetics by disruption of contiguous positive surface potential and charge reduction using alternate human framework

Romain Ollier, Aline Fuchs, Florence Gauye, Katarzyna Piorkowska, Sébastien Menant, Monisha Ratnam, Paolo Montanari, Florence Guilhot, Didier Phillipe, Mickael Audrain, Anne-Laure Egesipe, Damien Névoltris, Tamara Seredenina, Andrea Pfeifer, Marie Kosco-Vilbois & Tariq Afroz

To cite this article: Romain Ollier, Aline Fuchs, Florence Gauye, Katarzyna Piorkowska, Sébastien Menant, Monisha Ratnam, Paolo Montanari, Florence Guilhot, Didier Phillipe, Mickael Audrain, Anne-Laure Egesipe, Damien Névoltris, Tamara Seredenina, Andrea Pfeifer, Marie Kosco-Vilbois & Tariq Afroz (2023) Improved antibody pharmacokinetics by disruption of contiguous positive surface potential and charge reduction using alternate human framework, mAbs, 15:1, 2232087, DOI: 10.1080/19420862.2023.2232087

To link to this article: https://doi.org/10.1080/19420862.2023.2232087

© 2023 AC Immune SA, Lausanne, Switzerland. Published with license by Taylor & Francis Group, LLC.

View supplementary material

Published online: 05 Jul 2023.

Submit your article to this journal

Article views: 1268

View related articles

View Crossmark data

Full Terms & Conditions of access and use can be found at
https://www.tandfonline.com/action/journalInformation?journalCode=kmab20

MABS
2023, VOL. 15, NO. 1, 2232087
https://doi.org/10.1080/19420862.2023.2232087

Taylor & Francis
Taylor & Francis Group

REPORT

OPEN ACCESS Check for updates

Improved antibody pharmacokinetics by disruption of contiguous positive surface potential and charge reduction using alternate human framework

Romain Ollier[#], Aline Fuchs[#], Florence Gauye, Katarzyna Piorkowska, Sébastien Menant, Monisha Ratnam, Paolo Montanari, Florence Guilhot, Didier Phillipe, Mickael Audrain, Anne-Laure Egesipe, Damien Névoltris, Tamara Seredenina, Andrea Pfeifer, Marie Kosco-Vilbois, and Tariq Afroz

Research, AC Immune SA, Lausanne, Switzerland

ABSTRACT

Optimal pharmacokinetic (PK) properties of therapeutic monoclonal antibodies (mAbs) are essential to achieve the desired pharmacological benefits in patients. To accomplish this, we followed an approach comprising structure-based mAb charge engineering in conjunction with the use of relevant preclinical models to screen and select humanized candidates with PK suitable for clinical development. Murine mAb targeting TDP-43, ACI-5891, was humanized on a framework (VH1–3/VK2–30) selected based on the highest sequence homology. Since the initial humanized mAb (ACI-5891.1) presented a fast clearance in non-human primates (NHPs), reiteration of humanization on a less basic human framework (VH1-69-2/VK2–28) while retaining high sequence homology was performed. The resulting humanized variant, ACI-5891.9, presented a six-fold reduction in clearance in NHPs resulting in a significant increase in half-life. The observed reduced clearance of ACI-5891.9 was attributed not only to the overall reduction in isoelectric point (pI) by 2 units, but importantly to a more even surface potential. These data confirm the importance and contribution of surface charges to mAb disposition *in vivo*. Consistent low clearance of ACI-5891.9 in Tg32 mice, a human FcRn transgenic mouse model, further confirmed its utility for early assessment and prediction of human PK. These data demonstrate that mAb surface charge is an important parameter for consideration during the selection and screening of humanized candidates in addition to maintaining the other key physiochemical and target binding characteristics.

ARTICLE HISTORY
Received 27 March 2023
Revised 7 June 2023
Accepted 28 June 2023

KEYWORDS
antibody charge engineering; antibody developability; antibody disposition; Antibody humanization; antibody pharmacokinetics; FcRn transgenic mice; pharmacokinetic prediction

Introduction

Monoclonal antibodies (mAbs) have emerged as a major class of therapeutics for a wide range of medical applications. Despite the establishment of powerful *in vitro* technologies such as phage display or the creation of transgenic animals carrying human immunoglobulin genes, immunization of wildtype (WT) rodents remains a viable method to generate mAbs against challenging targets such as misfolded proteins or transmembrane receptors like G-protein coupled receptors (GPCRs).[1,2] Therefore, mAb humanization is still required in these cases and humanized mAbs continue to represent the majority of mAb-based products currently approved by the regulatory agencies.[3] The strategy and science of going from mouse to humanized sequences remain a cornerstone of the field. The first considerations focus on maximizing the heavy and light chain sequence identity to the human antibody repertoire, but the humanization process also permits further engineering to improve biophysical and physicochemical properties such as thermostability, colloidal stability or charge distribution.[4–8]

Optimal pharmacokinetics (PK) is an important aspect of the developability profile of a mAb to maximize its therapeutic benefits and minimize the risks of failure at later stages of development. The circulating half-life is even more critical to consider for therapeutic indications such as diseases of the central nervous system where high doses of mAbs are required to ensure sufficient exposure within the brain tissue.[2,9] Thus, developing a mAb with slow clearance is essential to maximize the needed exposure with the appropriate dosing regimen in patients. Typically, mAbs exhibit biphasic PK profiles following systemic administration. This is characterized by a rapid distribution phase followed by a slower elimination.[10] Slow clearance and long half-lives of mAbs result from their interaction with Fc neonatal receptor (FcRn), which enables the recycling of mAbs from the endosomal compartment to the extracellular space.[11] In fact, many studies have successfully exploited the FcRn recycling mechanism to further extend the half-life by Fc engineering to increase the binding affinity to FcRn.[12,13] Therefore, transgenic mice expressing the human FcRn (Tg32), recapitulating better the human FcRn recycling, are being increasingly used in the early stages of antibody discovery and development.[14] Interestingly, the eventual testing in humans of selected therapeutic mAbs has provided a better correlation of the PK parameters with those obtained in Tg32 mice as compared with non-human primates

CONTACT Romain Ollier romain.ollier@acimmune.com Research, AC Immune SA, EPFL Innovation Park, Building B, Lausanne 1015, Switzerland; Tariq Afroz tariq.afroz@acimmune.com Research, AC Immune SA, EPFL Innovation Park. Building G, Lausanne 1015, Switzerland

[#]These authors equally contributed to the manuscript.

Supplemental data for this article can be accessed online at https://doi.org/10.1080/19420862.2023.2232087

© 2023 AC Immune SA, Lausanne, Switzerland. Published with license by Taylor & Francis Group, LLC.
This is an Open Access article distributed under the terms of the Creative Commons Attribution-NonCommercial License (http://creativecommons.org/licenses/by-nc/4.0/), which permits unrestricted non-commercial use, distribution, and reproduction in any medium, provided the original work is properly cited. The terms on which this article has been published allow the posting of the Accepted Manuscript in a repository by the author(s) or with their consent.

(NHP).[15] This further confirms the utility of these transgenic mice for human PK prediction using allometric scaling.

Over the past two decades, our understanding of other factors influencing mAb disposition *in vivo* has significantly progressed. For example, fast-clearing mAbs with short half-lives are often associated with poor developability due to self-associations, nonspecific binding to extracellular proteins or uneven charge distribution.[16–19] Therefore, multiple *in vitro* assays have been established to de-risk the selection of candidates in order to exclude mAbs with higher risk of sub-optimal PK.[20–24] Despite the successful implementation of these screening assays in discovery workflows, limitations in predicting *in vivo* clearance remain, such that, for some candidates, engineering approaches are required to optimize for the desired PK profile.

To treat neurodegenerative disorders which are chronic, slow evolving diseases, an optimal PK profile is essential to allow sustained mAb exposure in the central nervous system when using immunotherapies. ACI-5891 was identified as an effective mAb to target TDP-43 in amyotrophic lateral sclerosis and frontotemporal dementia, two disorders mediated by pathological species of TDP-43.[25] TDP-43 functions intracellularly, mainly in the nucleus, to regulate gene transcription and RNA metabolism (e.g., splicing, processing, stability, translation and transport).[26] In the healthy, physiological state, TDP-43 has a modular structure with the N-terminal domain taking part in inter-molecular interactions for TDP-43 oligomerization.[27] The two RNA recognition motifs confer nucleic acid binding specificity whereas[28] the C-terminal region of the protein is involved in protein-protein interactions required for its function in RNA processing.[29] In disease, TDP-43 can acts as a 'prion-like' protein, misfolding into β-sheet structures that results in the aberrant accumulation with aggregate formation in the cytoplasm of affected neuron and glial cells.[30] Subsequent cell-to-cell propagation of TDP-43 pathology is mediated by transmission of misfolded seeding species.[31–33] Even though the structural features of extracellular seeding-competent TDP-43 remain to be deciphered, capture and clearance of these species by a mAb have been shown to significantly decrease pathological TDP-43 in animal models of these diseases.[25]

Here, we report engineering of ACI-5891.1, a humanized IgG1 mAb targeting TDP-43 that has an unexpected fast clearance in NHPs. Investigations into the short half-life of ACI-5891.1 and its original chimera ACI-5891.5 suggested the contribution of high positive surface potential in the variable fragments (Fvs) of the mAb. The original sequence, ACI-5891.5, was then rehumanized using an engineering approach focused on reducing positive charges in key areas and aiming for a more uniform charge distribution. Using *in silico* modeling, we identified a suitable pair of basic frameworks for complementarity-determining regions (CDR) grafting. This new scaffold enabled the disruption of positive surface potential while maintaining high binding affinity to TDP-43 and a high sequence identity to human germlines, thereby mitigating the likelihood of immunogenic reactions. The consequent engineered mAb, ACI-5891.9, demonstrated significant improvement in PK studies using both Tg32 mice and NHPs, confirming the utility of Tg32 mice to evaluate difference in charge variants. Furthermore, the predicted human clearance was consistent from both species providing a predicted human half-life of 27 to 30 days for ACI-5891.9. Taken together, the two non-clinical specie studies confirmed the highly favorable human PK profile of ACI-5891.9 post engineering to optimize the charge value and distribution.

Results

Fast clearance of ACI-5891.1, an anti-TDP-43 mAb humanized on framework VH1–3/VK2–30

To develop a therapeutic mAb targeting pathological TDP-43 in neurodegenerative diseases, a potent murine IgG2a mAb, ACI-5891, binding an epitope conserved across mouse, NHP and human in the TDP-43 C-terminal region, was identified by hybridoma technology.[25] In wildtype mice, ACI-5891 demonstrated a favorable half-life of 14 days in a single intravenous (IV) administration study at 30 mg/kg (Figure 1a, Supplementary Table S1) allowing assessment of functional efficacy in the mouse models of disease.[25] ACI-5891 was then humanized by choosing frameworks with the closest sequence identity to the mouse variable sequence. First, using the ACI-

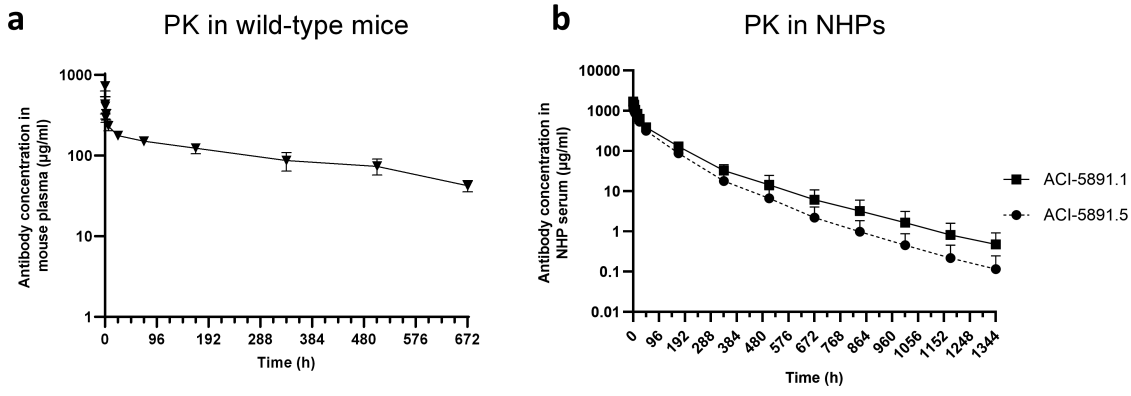

Figure 1. Pharmacokinetic profile of ACI-5891 variants in wildtype mice and NHPs. (a) ACI-5891 (mouse IgG2a) free plasma concentration (y-axis) over time (x-axis) in CD-1 mice after IV injection at 30 mg/kg. Data are depicted as the mean ± standard deviation for 3–4 animals/group. (b) Total serum concentration (y-axis) of human chimeric IgG1 ACI-5891.5 (solid circles) and humanized ACI-5891.1 (solid squares) over time (x-axis) in NHPs after IV bolus injection at 40 mg/kg. Data are depicted as the mean ± standard deviation for 3 animals/group.

5891 mouse Fv, a human IgG1 chimeric mAb, ACI-5891.5, was generated as reference. For humanization, CDRs were grafted onto the heavy and light chain variable frameworks, VH1–3 and VK2–30, respectively, and formatted as a human IgG1. The resulting humanized variant ACI-5891.1 had 87% and 88% identity to human VH and VL, respectively (Table 1). This was achieved while maintaining its high binding affinity to the target with a K_D of 175 pM as compared with the parental chimera, ACI-5891.5, that bound with a K_D of 328 pM (Table 1). Moreover, the thermostability of ACI-5891.1 was comparable to ACI-5891.5 demonstrated by the measured melting point (Tm) of the two mAbs (Table 1). However, a relatively short half-life of 4.6 and 4.0 days was observed for ACI-5891.1 and ACI-5891.5, respectively, following a single 40 mg/kg IV administration in NHP (Figure 1b, Table 2, Supplementary Figure S1a-b, Supplementary Table S2). Intriguingly, this resulted from fast clearance values of 0.497 and 0.716 mL/h/kg, for ACI-5891.1 and ACI-5891.5, respectively, while the volume of distribution was in the expected range for both mAbs (Table 2).

Investigation of factors contributing to fast clearance of ACI-5891.1

Following these unexpected findings, different factors impacting the fast clearance of an mAb were investigated, including FcRn binding, nonspecific binding, hydrophobicity, glycosylation profile, target-mediated drug disposition (TMDD) and charge. Both ACI-5891.1 and ACI-5891.5 demonstrated expected binding to human and NHP FcRn with fast association and dissociation kinetics at pH 6.0 and no residual binding at pH 7.4, suggesting a standard recycling behavior (Figure 2a, Table 1). In addition, ACI-5891 (murine IgG2a), ACI-5891.5 and ACI-5891.1 presented affinity ranging from 22–45 nM to mouse FcRn, demonstrating the expected higher affinity of IgGs for murine FcRn as compared to human FcRn (Table 3) and therefore the lack of PK translatability from WT mice to NHP. Next, the possibility of a potential nonspecific interaction and subsequent clearance with abundant negatively charged molecules present in the extracellular matrix such as heparin and insulin were tested. As compared to the positive and negative mAb controls, ACI-5891.1 and ACI-5891.5 demonstrated a low nonspecific score suggesting weak interaction with extracellular matrix components (Figure 2b). In addition, ACI-5891.1 demonstrated a low propensity for self-association, as the structural analysis of Fv model revealed the absence of large hydrophobic surface (Figure 2c), which was also confirmed by the low viscosity (3.0 cP) and absence of aggregation observed when concentrated at 120 mg/mL (data not shown). These data suggested that the hydrophobicity of ACI-5891.1 did not contribute to the observed clearance. Furthermore, for ACI-5891.1, the glycosylation profile and, more specifically, the high mannose content were within the expected range for therapeutic mAb (Table 4) and were unlikely to result in the observed clearance. Finally, to rule out TMDD, levels and localization of TDP-43 were measured in the blood of naive NHPs. The mean serum TDP-43 concentration in NHPs was 800 pg/mL (18 pM) (Supplementary Figure S2a). Even though ACI-5891.1 cross reacted with both human and cynomolgus monkey TDP-43 with high affinity, the serum concentration of target was 180-fold lower compared to the mAb concentration in serum at terminal time point (3.24 nM) in the NHP PK studies, suggesting that TMDD was not the mechanism contributing to the fast clearance. Moreover, no binding of ACI-5891.1 was observed on the plasma membrane on any blood cell, i.e., platelets, T cells, B cells, natural killer (NK) cells, monocytes, and erythrocytes by flow cytometry (Supplementary Figure S2b). Following permeabilization, expected intracellular binding was confirmed in T cells, B cells, NK cells, and monocytes (Supplementary Figure S2b). These data further rule out a role for TMDD of mAb via blood cell surface targeting.

Following evaluation and exclusion of all the above-mentioned factors influencing mAb clearance, we next hypothesized that the high positive charge of the chimera, ACI-5891.5, and the humanized variant, ACI-5891.1, may have contributed to the fast clearance observed in NHPs. In fact, the theoretical pI of ACI-5891.1 and ACI-5891.5 Fvs are 8.7 and 8.4, respectively (Table 1). These values are associated with net charge at pH 5.5 of + 10.1 and +

Table 1. Properties of ACI-5891 humanized variants.

Antibody	Human identity VH/VL (%)	Fv pI	Fv Charge pH5.5	Tm (°C)	TDP-43 K_D (pM)	FcRn affinity at pH 6.0 K_D (nM)	FcRn affinity at pH 7.4 K_D (nM)
ACI-5891.5	67/81	8.4	+10.0	72.0	328	505	No Binding
ACI-5891.1	87/88	8.7	+10.1	71.0	175	695	No Binding
ACI-5891.9	88/86	6.9	+4.3	70.6	126	865	No Binding

Fv: Fragment variable, pI: isoelectric point, Tm: melting temperature, DSF: differential scanning fluorimetry, SPR: Surface plasmon resonance.

Table 2. Population PK parameter estimates following single IV administration at 40 mg/kg in NHPs.

Parameters	Unit	ACI-5891.5	ACI-5891.1	ACI-5891.9
Cl	mL/h/kg	0.716	0.497	0.083
V_c	mL/kg	34.6	25.7	23.3
Q1	mL/h/kg	0.5	0.5	0.4
V_{p1}	mL/kg	33.7	31.2	12.3
Vd	mL/kg	68.3	56.9	35.6
$T_{1/2\ b}$	days	4.0	4.6	12.7

Cl:clearance from the central compartment, Vc: volume of the central compartment, Q1: intercompartment distribution clearance, Vp1: volume of the peripheral compartment, Vd: total volume of distribution = sum of Vc and Vp1, T1/2 b: terminal half-life.

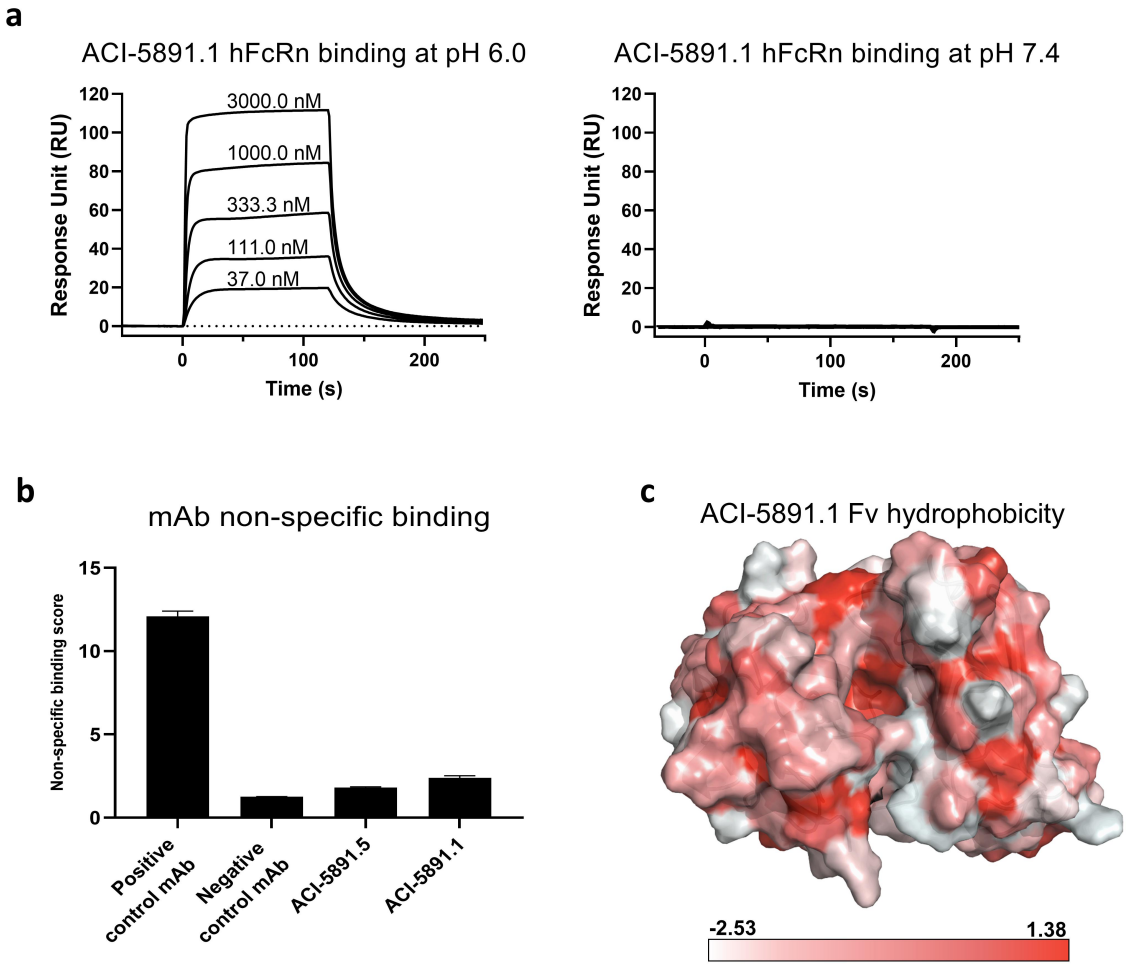

Figure 2. Investigation of factors contributing to fast clearance of ACI-5891.1. (a) Human FcRn (hFcRn) binding of ACI-5891.1 at pH 6.0 (left panel) and pH 7.4 (right panel). SPR measurement performed using antibody concentrations of 3000 nM, 1000 nM, 333.3 nM, 111.0 nM, and 37.0 nM as depicted. Sensorgrams are shown in black lines. (b) Non-specific binding of ACI-5891.1 and ACI-5891.5 by heparin and insulin ELISA. Mean signals for both targets are reported as nonspecific binding score. (c) Surface representation of ACI-5891.1 Fv model colored according to Eisenberg's scale of hydrophobicity (shown at the bottom of panel c). Intense red indicates the most hydrophobic residue while white represents the most hydrophilic residue.

Table 3. Affinity of ACI-5891 variants to mouse, human and NHP FcRn.

Antibody	Isotype	mFcRn affinity at pH 6.0 K_D (nM)	hFcRn affinity at pH 6.0 K_D (nM)	cFcRn affinity at pH 6.0 K_D (nM)
ACI-5891	Mouse IgG2a	45	N.B.	N.B.
ACI-5891.5	Human IgG1	22	505	512
ACI-5891.1	Human IgG1	29	695	749

N.B.: no binding, mFcRn (mouse), hFcRn (human), cFcRn (cynomolgus).

Table 4. Distribution of major glycoforms in ACI-5891.1 and ACI-5891.5.

Glycoform	ACI-5891.1	ACI-5891.5
G0F	64.1%	64.6%
G1F	15.6%	12.6%
G2F	1.4%	ND %
G0	4.8%	4.6%
M5	8.2%	5.5%

10.0, respectively (Table 1). More importantly, the analysis of the electrostatic surface potential of ACI-5891.5 Fv (identical to the original mouse mAb ACI-5891) molecular model revealed an uneven charge distribution, with substantial patches of positive charge resulting from contiguous basic residues from both framework and CDRs (Figure 3a). These observations supported further engineering focused on charge reduction and especially disruption of continuous positive surface potential while retaining mAb potency.

Generation of anti-TDP-43 humanized mAb, ACI-5891.9 with reduced charge using framework VH1-69-2/VK2–28

The original mouse CDRs were then humanized on a new framework selected for its intrinsic low isoelectric point value and ability to disrupt clusters of positive charges on ACI-5891 surface. Amongst VH germlines, VH1-69-2 was of particular interest because it exhibited a favorable charge profile with a pI value of 4.3 and net charge of −4.7 while having a percentage of sequence identity close to 65%

a

ACI-5891.5 Fv surface electrostatic potential

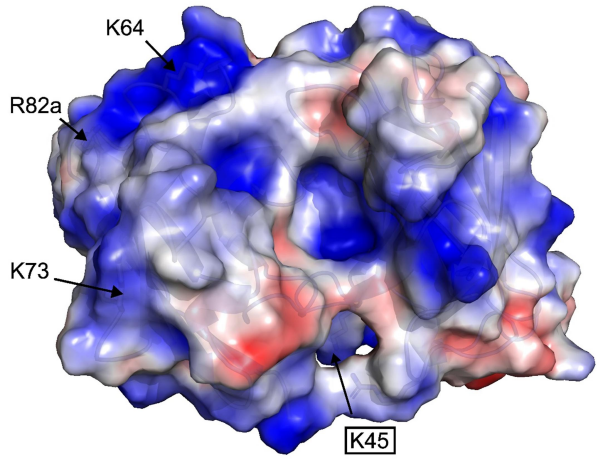

b

Sequence homology and charge profiles of selected human framework

VH germline	pI	Net Charge pH 5.5	% Identity
IGHV1-69-2	4.3	-4.7	64.3
IGHV1-24	4.7	-2.7	65.3
IGHV7-81	7.4	1.8	53.1
IGHV5-51	8.1	2.4	55.1
IGHV5-a	8.1	3	54.1
IGHV1-69	8.1	2.4	62.2
IGHV7-4-1	8.2	3.2	59.2
IGHV3-64	8.6	3.9	52
IGHV3-74	8.7	3.9	51
IGHV1-18	8.9	4.3	63.3
IGHV1-46	8.9	4.9	67.4
IGHV1-8	9	4.3	64.3
IGHV3-49	9	4.4	51
IGHV1-58	9.1	4.4	61.2
IGHV1-45	9.2	5.9	60.2
IGHV3-73	9.2	5.9	53.1
IGHV1-2	9.3	6.9	66.3
IGHV1-3	9.4	6.9	67.4

VL germline	pI	Net Charge pH 5.5	% Identity
IGKV2-40	4.1	-4.5	73.3
IGKV2D-40	4.1	-4.5	73.3
IGKV3D-20	4.4	-1.6	54.7
IGKV2-28	4.7	-1.1	72
IGKV2D-28	4.7	-1.1	72
IGKV4-1	4.7	-0.7	60.4
IGKV6D-41	4.7	-1	51
IGKV2D-29	5.4	-0.1	78
IGKV3D-7	5.9	0.3	52
IGKV2-29	6	0.5	80
IGKV3-20	6	0.4	55.8
IGKV3-11	6.1	0.4	51
IGKV3-7	6.5	0.9	51
IGKV2D-30	6.6	0.9	80
IGKV1-39	7.3	1.2	50
IGKV1D-39	7.3	1.2	50
IGKV3-15	7.4	1.3	50
IGKV3D-15	7.4	1.3	50
IGKV7-3	7.6	1.8	51
IGKV2-30	7.6	1.9	80
IGKV2-24	7.6	1.8	74
IGKV2D-24	7.9	1.8	74

Figure 3. Electrostatic surface representation of ACI-5891.5 Fv and selection of human framework (a) Electrostatic surface representation of ACI-5891.5 Fv model. Representation identical to the murine ACI-5891 Fv model. Key framework amino acids contributing to positive charges are indicated with white arrows. Positive charges are displayed in blue, negative charges in red, and neutral patches in white. Black box indicates light chain residue. (b) List of human VH and VL germlines with at least 50% sequence identity with original mouse sequences. Tables depict the calculated pI, the net charge at pH 5.5 and the sequence identity with the parental mouse antibody ACI-5891. Original germlines used for humanization of ACI-5891.1 are framed in blue and germlines selected for their lower charge are framed in red.

(Figure 3b). From the analysis of VL human germlines amino acid sequences, VK2–40 and VK2–28 presented the lowest charge values and the best sequence identity to ACI-5891 VL. When performing the *in-silico* modeling of ACI-5891 CDR grafting, only frameworks VH1-69-2 and VK2–28 could reduce significantly the Fv net charge. Indeed, the use of VH1-69-2 as human acceptor framework disrupted a large patch of positive charges by replacing murine positively charged residues with substitutions K64Q, R82aS and K73T (Figure 3a). In addition, the use of germline, VK2–28, contributed to the charge reduction with substitution K45Q in the VL framework 2. The net charge of the resulting humanized mAb, ACI-5891.9, was reduced to + 4.3 and the Fv theoretical pI decreased to 6.9 (Table 1). Moreover, the electrostatic surface potential representations (Figure 4) indicate that the charge reduction was associated with a more balanced charge distribution across the molecular surface of ACI-5891.9 compared to ACI-5891.5 and ACI-5891.1. Importantly, this was achieved while maintaining the high identity to human VH/VL germlines in addition to the target binding affinity (Figure 5, Table 1). The stability of all three mAbs measured by differential scanning fluorimetry (DSF) was above 70°C as expected for a human IgG1. The measured affinity of ACI-5891.9 to human FcRn at pH 6.0 was comparable to ACI-5891.5 and ACI-5891.1 with no residual binding observed at pH 7.4 (Table 1).

Significant reduction in clearance and increase in half-life of ACI-5891.9

To assess the impact of charge reduction and the concomitant disruption of positive charge surface in the humanized variant ACI-5891.9, PK studies were first conducted in Tg32 mice (Figure 6a, Table 5, Supplementary Figure S3a-c, Supplementary Table S3). The chimeric mAb together with the two humanized variants ACI-5891.1 and ACI-5891.9 were administered at single doses of 40 mg/kg IV each. ACI-5891.9 had a clearance of 0.183 mL/h/kg, which was significantly lower than ACI-5891.5 and ACI-5891.1, with clearances of 0.235 mL/h/kg and 0.428 mL/h/kg, respectively. The reduced clearance of ACI-5891.9 translated in a half-life of 16.4 days while the chimera ACI-5891.5 and the humanized ACI-5891.1 presented shorter half-life of 9.6 and 10.8 days, respectively. The volume of distribution of ACI-5891.5 was comparable to that of ACI-5891.9 but was higher for ACI-5891.1 (Table 5). Therefore, the resulting half-life reflected the interplay between clearance and volume of distribution. For ACI-5891.1, a sharp decline in mean PK profile observed at later time points from 21 days post-administration was potentially attributed to an anti-drug antibody response in a subset of mice. The sparse sampling used in the study, where each animal was bled only once or twice, limits conclusions that could be drawn from such PK profile. Consistent with data from Tg32 mice, ACI-

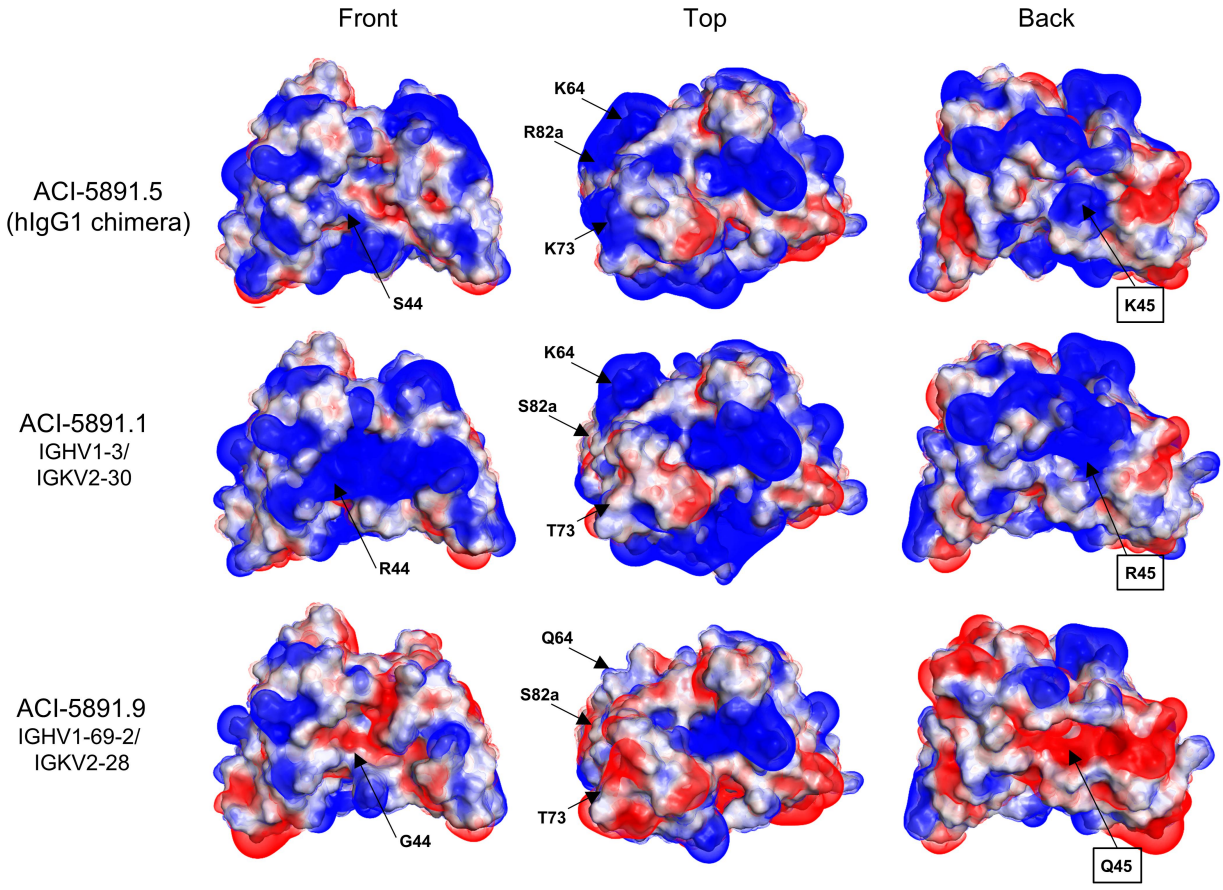

Figure 4. Electrostatic surface representation of ACI-5891 humanized variants. Front, top, and back view of ACI-5891 chimera (ACI-5891.5), and the variants: ACI-5891.1 and ACI-5891.9, humanized using IGHV1–3/IGKV2–30 and IGHV1-69-2/IGKV2–28, respectively. Positive charges are displayed in blue, negative charges in red, and neutral patches in white. Black boxes indicate light chain residue.

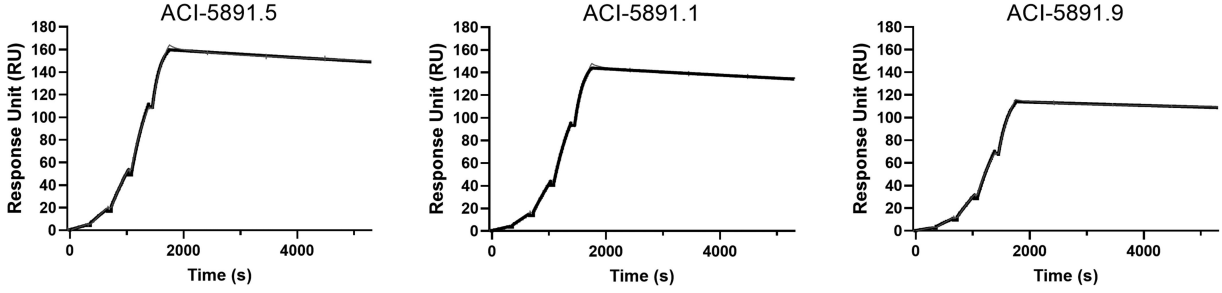

Figure 5. Binding kinetics of ACI-5891 variants determined by SPR. Affinity determination of ACI-5891 variants to TDP-43 by SPR in single cycle kinetics at concentration ranging from 1.2 nM to 100 nM. Analysis was performed using a 1:1 binding model. Gray line depicts the experimental data and black line depicts the data fit to the model.

5891.9 exhibited a significantly reduced clearance of 0.083 mL/h/kg in NHP, which was more than five times lower compared to the ACI-5891.1 (0.497 mL/h/kg) (Figure 6b, Table 2, Supplementary Figure S1c, Supplementary Table S2). Consequently, the half-life in NHP increased from 4.6 for ACI-5891.1 to 12.7 days for ACI-5891.9 (Table 2). Taken together, the data from Tg32 mice and NHPs confirmed that the observed significant decrease in mAb clearance resulted from the selection of alternate framework VH1-69-2/VK2–28 that lowered overall charge and disrupted the contiguous positive surface potential of ACI-5891.

ACI-5891.9 demonstrates predicted human PK suitable for clinical development

NHPs and Tg32 mice are two relevant preclinical models that aid in the prediction of mAb clearance in humans. Using allometric scaling, the predicted mAb clearance in humans based on the PK data in Tg32 mice and NHPs was 0.195 mL/h/kg and 0.256 mL/h/kg for ACI-5891.1 versus 0.082 mL/h/kg and 0.043 mL/h/kg for ACI-5891.9, respectively (Supplementary Table S4). The predicted human clearance was consistent from both species providing values within a 2-fold difference. These data resulted in a predicted human half-life of 27 to 30 days for ACI-

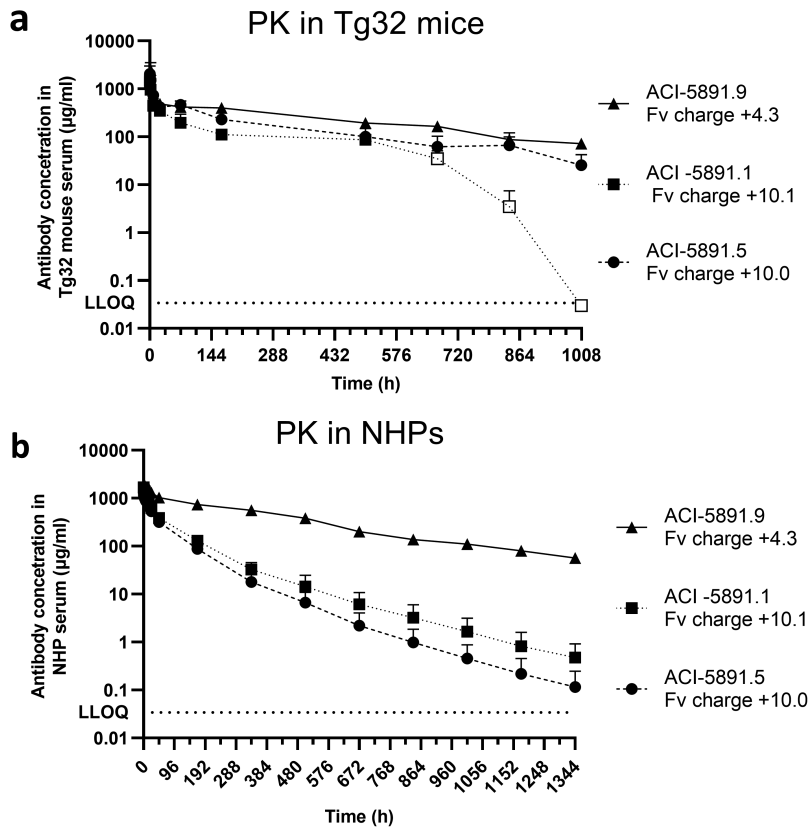

Figure 6. Single-dose pharmacokinetics in Tg32 mice and NHPs. (a) Total antibody serum concentration (y-axis) of ACI-5891.5, ACI-5891.1 and ACI-5891.9 over time (x-axis) in Tg32 mice after IV bolus injection at 40 mg/kg. Data are depicted as the mean ± standard deviation for 3 animals/time point, for a total of 21 animals per group. Empty symbols represent data point for which at least one serum concentration was below the limit of quantification. (b) Total antibody serum concentration (y-axis) of ACI-5891.5, ACI-5891.1 and ACI-5891.9 over time (x-axis) in NHPs after IV bolus injection at 40 mg/kg. Data are depicted as the mean ± standard deviation for 3–4 animals/group. Lower limit of quantification (LLOQ) indicated in dotted line for both graphs.

Table 5. Population PK parameters estimates following single IV administration at 40 mg/kg in Tg32 mice.

Parameters	Unit	ACI-5891.5	ACI-5891.1	ACI-5891.9
Cl	mL/h/kg	0.235	0.428	0.183
V_c	mL/kg	18.8	29.3	20.8
Q1	mL/h/kg	2.8	2.4	2.8
V_{p1}	mL/kg	55.6	114.7	79.0
Vd	mL/kg	74.4	144.0	99.8
$T_{1/2\ b}$	days	9.6	10.8	16.4

Cl:clearance from the central compartment, Vc: volume of the central compartment, Q1: inter-compartment distribution clearance, Vp1: volume of the peripheral compartment, Vd: total volume of distribution = sum of Vc and Vp1, T1/2 b: terminal half-life.

5891.9 versus 17 to 22 days for ACI-5891.1, respectively, and confirming the highly favorable human PK profile of ACI-5891.9.

Discussion

In this report, we present our approach to generate and select a humanized mAb targeting TDP-43 with desired potency and exposure *in vivo*. These data demonstrate the relevance of our humanization process to optimize mAb surface charge that significantly ameliorated the mAb PK profile in *vivo*. This was achieved by selection of an appropriate human framework based on sequence identity and physicochemical properties to minimize the risks of immunogenicity in humans. Finally, considering the limitations of the current *in vitro* assays to de-risk the selection of candidates with sub-optimal PK, the Tg32 mice appears to be a suitable model for both NHP and human PK predictions.

The observed clearance in NHPs for ACI-5891.1 (0.497 mL/h/kg) and ACI-5891.5 (0.716 mL/h/kg) was 2–3-fold higher than the reported range of 0.24–0.30 mL/h/kg (95% confidence interval) based on a population PK analysis of mAbs in NHPs.[34] Several lines of evidence suggested that there was a minimal contribution of TMDD to fast clearance. Firstly, even though TDP-43 could be measured in healthy NHP and human plasma,[35] the levels were very low compared to the antibody levels measured in the PK studies. Moreover, being mainly an intracellular protein, this pool of soluble TDP-43 most likely represented cell turnover. Finally, ACI-5891.9 binding with high affinity to

human and NHP TDP-43 (similar to ACI-5891.1) showed low clearance, demonstrating lack of TMDD as a major contributor to clearance mechanism. Surprisingly, none of the previously reported *in vitro* assays predicted fast clearance for ACI-5891.1, suggesting inherent limitations in their versatility to identify and de-risk the selection of sub-optimal candidates. Reiteration of humanization using a less basic framework while preserving sequence identity confirmed the contribution of positive surface potential to the fast clearance of ACI-5891.1 and ACI-5891.5, suggesting that charge-mediated interactions are not well detected in available *in vitro* assays to assess characteristics influencing nonspecific clearance.

The change of humanization framework from VH1–3/VK2–30 to a less basic VH1-69-2/VK2–28 resulted in a reduction of overall charge as well as an intended disruption to the large positive surface potential. The framework residues, K64, R82a, K73 (in the heavy chain) and K45 (in the light chain), comprised a contiguous positive surface potential in ACI-5891.5 Fv. Even though this positive surface was partially reduced in ACI-5891.1 (R82aS, K73T), basic framework residues such as R44 (in the heavy chain) compensated to retain the high positive charge and created new positive surface potential. Strikingly, by using germlines, VH1-69-2/VK2–28, less basic framework residues such as Q64, G44 and Q45 were introduced to completely disrupt the large positive surface potential. This charge removal was achieved with minimal changes in the framework region, thus reducing the risk of immunogenic epitopes by preserving natural sequences of human germlines. ACI-5891.9 frameworks have 100% identity with VH1-69-2 while three back-mutations were introduced in VK2–28 to preserve binding affinity to TDP-43. Moreover, this change resulted in a significant reduction of charge by 5.8 units in ACI-5891.9 that translated in a six-fold reduction of clearance in NHPs as compared with ACI-5891.1 (Table 2). In fact, the measured clearance of ACI-5891.9 (0.083 mL/h/kg) was even lower than the typical clearance of 0.24–0.30 mL/h/kg reported by Betts *et al.* [34] Our data are consistent with the hypothesis that mAbs with Fv net charge superior to + 6.2 (at pH 5.5) have higher risk of fast nonspecific clearance in NHPs.[23] These data demonstrate that for ACI-5891, the change of the Fv charge from + 10.1 to + 4.3 was sufficient to see a significant decrease in mAb clearance *in vivo* even though it is difficult to infer the relative contributions of charge distribution vs. total net charge in reducing clearance.

These data emphasize that while sequence identity, stability and expression are parameters generally considered for selecting human acceptor frameworks, charge should be equally evaluated during this selection. Therapeutic antibodies with high positive charges have been shown to be more susceptible to interact with the negatively charged extracellular matrix and cell membrane, and consequently more likely to be cleared via pinocytosis.[36,37] While the correlation between charge and clearance has been demonstrated for a given mAb, studies performed on a larger and more diverse set of mAbs suggested otherwise, illustrating a complex relationship.[5,20,38] Several studies have even highlighted the limitations of charge reduction on mAb disposition, and the principles could not be universally applied.[39] Recently, Liu et al.[36] observed a "U"-shaped relationship between nonspecific clearance and mAb charges, claiming an increased clearance at both very high and low charges, suggesting only a narrow optimal charge range in which, interestingly, ACI-5891.9 would fall. Therefore, the use of an appropriate rodent model recapitulating good inter-species translatability is essential for screening charge variants prior to evaluation in NHP. The PK data generated with the original murine IgG2a antibody demonstrated the lack of predictability for the fast clearance observed with the chimeric antibody in NHP or Tg32 mice. This can be explained by the differences in affinity of antibodies for FcRn across species. While the recycling mechanism is similar across species, human and rodent antibodies have a high affinity to rodent FcRn as compared with that of NHPs and human, leading to poor PK translatability from WT mice.[40,41] In this study, Tg32 mice were confirmed as a suitable model that could be used to screen and exclude mAbs with a risk of poor PK profile prior to testing in NHPs as both species efficiently discriminated between the different ACI-5891 charge variants. Our data confirmed that the human PK predicted for ACI-5891.9 was consistent when scaled from both Tg32 mice and NHPs and significantly better than the one obtained for ACI-5891.1 (Supplementary Table S4).

Together, these data confirm that charge engineering can substantially improve the developability of a clinical candidate. Furthermore, our comparative studies demonstrate the utility of Tg32 mice to investigate the effect of charge engineering on mAb PK, offering alternatives to using studies with primates to achieve the same goal.

Material and methods

Antibody production and purification

The Fv domain of ACI-5891 was discovered by hybridoma technology, from mice immunized using the SupraAntigen® vaccine technology.[25] VH and VL domains of ACI-5891 variants were cloned into mammalian expression vectors containing the human kappa constant domain and the human IgG1 constant domain, respectively. Chinese hamster ovary cells were transiently transfected with equimolar quantities of heavy and light chain vectors. Antibodies were purified from supernatants by protein A chromatography (Cytiva, cat# 17543803). The identity and purity of the purified antibodies were confirmed using native and reduced SDS-PAGE. Concentrations of antibodies were measured using the NanoDrop Spectrophotometer (Thermo Fisher Scientific).

Humanization of murine ACI-5891

The murine ACI-5891 was humanized by CDR grafting. CDRs were identified according to the Kabat nomenclature. First, structural models of Fv domains were generated using the AbodyBuilder pipeline and the APBS program used to calculate the electrostatic potential which was then rendered in Pymol (Schrodinger).[42] Hydrophobicity of ACI-5891 was analyzed using the surface representation of ACI-5891 molecular model colored according to the Eisenberg scale of

hydrophobicity scale.[43] The theoretical pI and charge of Fv domains were determined using the prediction server Isoelectric Point Calculator 2.0,[44] reporting the average predicted pI and net charge at pH5.5. Human heavy and light chain framework sequences were identified from the IMGT antibody database based on sequence identity. Theoretical pI of individual VH and VL germline were calculated as previously described. Murine CDRs of ACI-5891 VH and VL were grafted onto selected frameworks VH1–3/VK2–30 and VH1-69-2/VK2–28 to generate ACI-5891.1 and ACI-5891.9, respectively. Back-mutations were introduced at critical framework residues known to influence CDR conformation and based on the molecular model of ACI-5891 Fv domains.[45]

Binding affinity measurement by surface plasmon resonance

Affinity measurement to human FcRn

Binding affinities of ACI-5891 variants to human FcRn (hFcRn) were measured at pH 6.0 and pH 7.4 by surface plasmon resonance (SPR) using a Biacore 8K instrument (Cytiva). Biotinylated hFcRn (AcroBiosystems, cat # FCM-H82W4) was immobilized on flow-cell 2 (fc2) of flow-channels 1 to 8 of a streptavidin (SA) sensor chip (Cytiva, cat# BR-1005-31) to reach a final surface density of approximatively 150 RU. For K_D determination, recombinant mAbs diluted in the matching running buffer (either PBS-P+ pH 6.0 or PBS-P+ pH 7.4) were flowed over the immobilized hFcRn at five different concentrations ranging from 3000 nM to 37 nM from a three-fold serial dilution. Kinetic measurements were performed with a contact time of 120 s and a dissociation time of 120 s at a flow rate of 30 µL/min. Regeneration was performed using two consecutive injections of PBS-P+ pH 7.4 for 30 s. Sensorgrams obtained from multi-cycle kinetics were double-referenced using the blank fc1 and blank injections and analyzed with a steady-state affinity model using the Biacore Insight evaluation software.

Affinity measurements to human TDP-43

Target binding affinities were performed on a Biacore 8K instrument (Cytiva). Recombinant human TDP-43 N-terminally fused to a SUMO tag (Selvita) was immobilized on flow-cells 1 and 2 of channels 1 to 8 of a CM5 sensor chip (Cytiva, cat# BR100530) to reach 300 to 400 RU on all eight channels. Increasing concentration of recombinant mAbs ranging from 1.2 to 100 nM prepared from a three-fold serial dilution in running buffer were injected in single-cycle kinetics on fc1 and fc2. Kinetic measurements were performed with a contact time of 300 s and a dissociation time of 3600 s at a flow rate of 30 µL/min. Regeneration was performed using two consecutive injections of 10 mM glycine-HCl pH 1.7, at a flow rate of 30 µL/min for 30 s. Results obtained from single-cycle kinetics were double-referenced using the blank fc1 and evaluated the Biacore Insight evaluation software. Sensorgrams were analyzed using the 1:1 binding fit model with variable reflective index and global Rmax parameters.

Thermostability measurement by DSF

The melting temperatures (Tm) were determined using a QuantStudio™ 3 Real-Time PCR System (Thermo Fisher Scientific). Measurements were performed by mixing 5 µg of antibody diluted in protein thermal shift assay buffer (Thermo Fisher Scientific, cat#4461146) with 2 µL of 5×Protein Thermal Shift Dye (Thermo Fisher Scientific, cat#4461146) in a final volume of 20 µL/well. The plate was scanned from 25°C to 100°C at a rate of 0.05°C/s. The first Tm was assigned using the first derivative of the raw data calculated with the protein thermal shift analysis software (Thermo Fisher Scientific).

Glycosylation profile

Recombinant antibodies were analyzed by quick N-glycan method to detect the proportion of N glycan forms. Samples were reduced using 20 mM dithiothreitol (DTT) and incubated for 30 min at room temperature (RT). The resulting preparation was separated on reverse-phase column (Agilent, cat# PL1912–1502) using an elution gradient of buffer A (0.1% trifluoroacetic acid (TFA) in water) and buffer B (0.1% TFA in acetonitrile), liquid chromatography – mass spectrometry (LC-MS) analysis was performed on a Q-TOF mass spectrometer (Agilent)

Data deconvolution was performed using the Agilent bioconfirm software and each N-glycan type was manually determined by matching the measured mass to the theoretical mass. The relative abundance of glycan forms was calculated by dividing the intensity of each peak to the total peak intensity.

Determination of monomer content by SE-HPLC

For size exclusion – HPLC (SE-HPLC) analysis, 15 µL of sample was injected on a TSK gel G3000 SWXL (Merck, cat# 808541) using a HPLC system (Waters, 2695 separation module). Samples were run in 1× PBS at 1 mL/min and 30°C. Elution was monitored at 280 nm using a UV detector (Waters, 2998 Photodiode Array Detector). Data were analyzed using Empower 3 software and expressed as percent of peak area over total area.

Insulin and heparin ELISA

The nonspecific binding of humanized variants was tested in ELISA, adapted from assays described previously,[19,24] using insulin and heparin as coating agent. Briefly, insulin (Sigma-Aldrich, cat# I9278) at 5 µg/mL and heparin (Sigma-Aldrich, cat# H3149) at 10 µg/mL were coated onto ELISA plates (Thermo Fisher Scientific, cat#442404) at 50 µL/well overnight at 4°C or RT, respectively. Wells were blocked with 150 µL of PBS containing 0.5% bovine serum albumin (BSA) for 1 h at RT. Plates were washed three times with PBS buffer containing 0.1% Tween 20, and 50 µL of recombinant antibodies diluted to 100 nM in PBS containing 0.5% BSA were added to each well in triplicate. A blank control with no antibody was included for background normalization. Positive and negative control human IgG1 antibodies, previously described in Jain et al.,[46] were included for reference. After 1 h incubation at RT,

plates were washed as described above. Bound antibodies were detected with 50 µL/well of an anti-human IgG conjugated to horseradish peroxidase (Abcam, cat# ab98624) diluted to 1/10,000 in PBS with 0.1% Tween 20. Plates were incubated for 30 min at RT and washed as described above. Finally, 50 µL of TMB substrate (BD Biosciences, cat# 555214) was added to each well and incubated for 10–15 min. Reactions were stopped by adding 50 µL of 2 M HCl to each well. The absorbance was read at 450 nm and the binding score to individual antigen determined by normalizing absorbance with control wells without test antibody. The reported nonspecific binding score is the average of individual scores.

Pharmacokinetic study in wildtype mice

The *in vivo* study was approved by the Institutional Animal Care and Use Committee (IACUC) of WuXi AppTec and performed in an accredited animal facility. Nine female CD-1 mice (age: 6–8 weeks) were used in this study. Animals were purchased from Hilltop Lab Animals, Inc. Free plasma concentrations of ACI-5891 were determined after single intravenous administrations at 30 mg/kg of ACI-5891. Plasma was collected in each animal from the tail vein on five occasions. Plasma samples were collected from 3 mice per time-point after dose administration at the following time-points: 0.05 h, 0.25 h, 0.5 h, 1 h, 2 h, 6 h, 24 h, 72 h and day 7, day 14, day 21 and day 28.

Pharmacokinetic study in non-human primates

The *in vivo* study was approved by the IACUC of WuXi AppTec and performed in an animal facility accredited by the provincial animal management office. Male cynomolgus monkeys ≥2 years old, weighing ≥2 kg, were purchased from Hainan Jingang Laboratory Animal Co. Ltd. All tested antibodies were administered by single IV bolus injection at 40 mg/kg ($n = 4$ animals per dose group and per antibody). Serum was collected in each animal at the following timepoints: pre-dose, 0.05 h, 1 h, 2 h, 4 h, 8 h, 16 h, 24 h, 48 h, day 7, day 14, day 21, day 28, day 35, day 42, day 48, day 56.

Determination of human antibody concentration in NHP serum

The total concentration of human antibody in cynomolgus monkey serum was determined by ELISA. A biotinylated mouse polyclonal anti-human Kappa chain antibody (Southern Biotech, cat#SBA-2064-08) diluted to 1.5 µg/ml in PBS with 0.05% Tween 20 was captured onto a streptavidin coated microplate (Microcoat Biotechnologie GmbH, cat# 604500) for 1 h at RT. Plates were washed four times with PBS with 0.05% Tween 20 and blocked with 100 µl of PBS with 1% BSA and 0.05% Tween 20 (dilution buffer) for 1 h at RT. Standard curves prepared from a two-fold serial dilution starting at 50 ng/mL and test samples diluted in 1:100 in dilution buffer supplemented with 1% cynomolgus monkey serum (Neo-Biotech) were loaded to the plates, incubated for 90 min at RT, and washed as previously described. Bound human antibodies were detected with an anti-human Kappa chain antibody conjugated to horseradish peroxidase (Southern Biotech, cat# SBA-9230-05) diluted to 4.0 ng/ml in dilution buffer. Plates were incubated for 30 min at RT and washed as previously described. Finally, TMB substrate (SeraCare, cat# 5120–0081) was added to each well and incubated for 10–15 min. Reactions were stopped by adding 100 µL of Stop solution (Bethyl, cat#E115) to each well. Absorbance was read at 450 nm with a reference wavelength at 690 nm using a Biotek microplate reader. Concentrations of all serum samples were back-calculated against a reference standard using a non-linear 4-parameter regression fit including a 1/y2 weighting.

Quantification of TDP-43 in NHP serum

TDP-43 levels in cynomolgus monkey serum were determined by immunoassay based on single molecule array (SIMOA®) technology using AC Immune's proprietary anti-TDP-43 mAbs. For capture, an AC Immune proprietary murine anti-human TDP-43 mAb was conjugated with Quanterix paramagnetic carboxylated beads according to the manufacturer's instructions. Briefly, beads were washed and activated with ice-cold 1-ethyl-3-[3-dimethylaminopropyl]carbodiimide] for 30 minutes at 4°C. Activated beads were incubated with the murine antibody in PBS 1× (0.2 mg/mL) for two hours at 4°C with shaking. The beads were washed several times and blocked with Quanterix bead blocking buffer according to the manufacturer's instructions. A final heat treatment step was performed to improve the stability of the beads by incubating the beads at 37°C for 18 hours with shaking. For detection, TDP-43 mAb ACI-5891 (murine IgG2a) was biotinylated using the Thermo Fisher Scientific EZ-Link NHS-PEG4 Biotin Kit. According to the manufacturer's instructions, 6 µL of biotin solution was used for 0.2 mg of antibody. Several steps of buffer exchange and purification in PBS 1× were performed using the Amicon Ultra-0.5 Centrifugal Filter Unit. For the assay, a Simoa® microplate shaker from Quanterix was used with constant shaking at 800 rpm according to the manufacturer's instructions. Briefly, a 96-well plate (96-Well Polypropylene Microplates, 249944, Thermo Fisher Scientific) was loaded with 100 µL of diluted serum (1/10) and 25 µL of antibody conjugated beads (0.02×109 beads/mL final concentration). After incubation of this mixture for 30 minutes, the plate was washed and 100 µL of 0.3 µg/mL biotinylated ACI-5891 was added to the wells and incubated for 10 minutes. Streptavidin-β-galactosidase (SBG) diluted to 150 pM in SBG diluent was then added and incubated for 10 minutes. The beads were then resuspended in a resorufin-β-D-galactopyranoside substrate, transferred to the Simoa® disc and the fluorescence signal measured. Data were calculated using SR-X software to obtain raw data expressed as average enzyme per bead (AEB). Samples were tested in duplicate. The calibration curve was generated using recombinant human TDP-43 N-terminally fused to a SUMO tag (Selvita) diluted to a concentration range of 0.98 to 4,000 pg/mL.

Measurement of TDP-43 expression in NHP peripheral whole blood

Fresh whole blood from naive NHPs in K_2EDTA anticoagulant were used and a combination of monoclonal antibodies to detect T, B and NK cells, erythrocytes, monocytes and platelets was used for immunophenotyping (Supplementary Table S5). Intracellular staining for TDP-43 was performed after detergent-based permeabilization, whereas extracellular staining was performed directly on live, non-permeabilized cells. ACI-5891.1 was labeled with Alexa Fluor 647 dye. A secondary fluorescent antibody AF647 was used as a control. This condition was defined as fluorescence minus one (FMO) and was used to determine the background level of fluorescence for all given markers within the panel for normalization. The percentages of each cell population measured using the full panel and the FMO samples were compared. Sample acquisition was performed using an 8-color (triple laser) BD FACSCanto II cytometer running BD FACSDiva software (version 6.1 BD Biosciences). To correct for the spectral overlap of the fluorochromes in the analysis, a series of monochromatic compensation samples were prepared and analyzed using beads. The spectral overlaps generated in each detector for these samples were automatically calculated by the instrument software and used to generate a compensation matrix for the analysis. The final settings (voltages and compensation matrix) were applied to all sample analysis protocols and panels. This compensation procedure was performed on each analysis occasion.

Pharmacokinetic study in Tg32 mice

The *in vivo* study was approved by the project license holder under the UK home office project license No. PPL PP9376768 and conducted in a facility approved by the UK home office (Establishment License X5CB0078). For each antibody, 21 male hFcRn Tg32 homozygous transgenic mice were used (Jackson Laboratory, Strain #:014565). Animals were housed and maintained according to the procedures established by Charles River Laboratories, Edinburgh Ltd. Test articles were administered by single IV bolus in saphenous vein at 40 mg/kg. Animals were sparse sampled. Serum was collected from each animal on a maximum of two occasions. Three serum samples were obtained at each timepoint at the following time points: 0.083 h, 0.25 h, 2 h, 8 h, 24 h, 72 h and day 7, day 14, day 21, day 28, day 35, day 42.

Determination of human antibody concentration in Tg32 mice serum

The total concentration of human antibody in mouse serum was determined by ELISA. A biotinylated mouse monoclonal anti-human IgG (Abcam, cat#256120) diluted to 0.75 µg/mL in PBS containing 0.05% Tween 20 was captured onto a streptavidin coated microplate (Microcoat Biotechnologie, cat# 604500) for 1 h at RT. Plates were washed four times with PBS containing 0.05% Tween 20 and blocked with 100 µL of PBS containing 1% BSA and 0.05% Tween 20 (dilution buffer) for 1 h at RT. Standard curves prepared from a two-fold serial dilution starting at 22 ng/mL and test samples diluted 1:100 in dilution buffer supplemented with 1% mouse serum (BioIVT) were loaded to the plates, incubated for 90 min at RT and washed as previously described. Bound human antibodies were detected using an anti-human Kappa chain antibody conjugated to horseradish peroxidase (Southern Biotech, cat# SBA-9230-05) diluted to 3.2 ng/mL in dilution buffer. Plates were incubated for 30 min at RT and washed as described above. Finally, TMB substrate (SeraCare) was added to each well and incubated for 10–15 min. Reactions were stopped by adding Stop solution (Bethyl) to each well. Absorbance was read at 450 nm with a reference wavelength at 690 nm using a Biotek microplate reader. Concentrations of all serum samples were back-calculated against a reference standard using a non-linear 4-parameter regression fit including a 1/y2 weighting.

Pharmacokinetic data analysis

Plasma concentration-time profiles were used to determine PK parameters and half-life in CD-1 mice using non-compartmental analysis (Phoenix WinNonlin, version 6.3; Pharsight Corporation). For Tg32 mice and NHPs, PK parameters were estimated by non-linear mixed effect (NLME) modeling. A 2-compartmental model with linear elimination from central compartment was systematically assessed. NHP with confirmed anti-drug antibody were excluded from PK analysis (1 animal for ACI-5891.1 and 1 animal for ACI-5891.5). In Tg32 mice study, concentration at time points showing potential sign of anti-drug antibody response for ACI-5891.1 and ACI5891.5 (unexpected concentration drop in some animals from 504 h) were excluded from PK analysis. Only the linear portion of the PK profile was used to assess clearance for 5891.1. In the final model, omegas were fixed to 0.1 for all PK parameters, to enable the use of Stochastic Approximation Expectation Maximization (SAEM) algorithm, except ACI-5891.1 in NHP where omega was identifiable on CL and Vp1.

PK parameters are reported as typical population PK parameters and the terminal half-life is derived from it. To evaluate the final PK models, visual predictive checks were performed by simulations based on the final PK estimates using 1000 individuals. Mean prediction concentrations with their 95% percentile interval are plotted and compared with observed data (see Supplementary Figures S1, 3). The population PK parameters describing the PK in Tg32 mice and NHPs for each tested antibody were scaled by allometric scaling using single species fixed exponent from Tg32 mice and NHPs to predict human PK parameters. Exponent estimated by Betts et al.[34] were used for the prediction of human linear PK of mAbs. Data preparation, exploration and model pre- and post-processing was performed with Rstudio (3.6.3) and the R package IQRtools (1.8.0, IntiQuan). Parameters for NLME models were estimated using Monolix (2019R1, Lixoft).

Acknowledgments

We thank Drs Anita Hamilton and Tim D. Jones for their expert advice during the humanization of ACI-5891.

Disclosure statement

No potential conflict of interest was reported by the author(s).

Funding

This study was funded by AC Immune SA.

Abbreviations

CDR	Complementarity-determining regions
Cl	Clearance from the central compartment
DSF	Differential scanning fluorimetry
ELISA	Enzyme-Linked Immunosorbent Assay
Fc	Fragment crystallizable
fc	flow cell
FcRn	Fc neonatal receptor
hFcRn	Human Fc neonatal receptor
Fv	Fragment variable
GPCR	G-protein coupled receptors
IgG	Immunoglobulin
IV	Intravenous
LLOQ	Lower limit of quantification
mAb	Monoclonal antibodies
NHP	Non-human primates
NK	Natural killer
pI	Isoelectric point
PK	Pharmacokinetic
Q1	Inter-compartment distribution clearance
RU	Response unit
SPR	Surface plasmon resonance
$T_{1/2\ b}$	Terminal half-life
TDP-43	TAR DNA-binding protein 43
Tm	Melting temperature
TMDD	Target mediated drug disposition
V_c	Volume of the central compartment
VH	Variable Heavy chain
VL	Variable Light chain
V_{p1}	Volume of the peripheral compartment
WT	Wildtype

References

1. Ju MS, Jung ST. Antigen design for successful isolation of highly challenging therapeutic anti-GPCR antibodies. Int J Mol Sci. 2020;21:8240. doi:10.3390/ijms21218240. PMID: 33153215.
2. Plotkin SS, Cashman NR. Passive immunotherapies targeting Abeta and tau in Alzheimer's disease. Neurobiol Dis. 2020;144:105010. doi:10.1016/j.nbd.2020.105010. PMID: 32682954.
3. Lyu X, Zhao Q, Hui J, Wang T, Lin M, Wang K, Zhang J, Shentu J, Dalby PA, Zhang H, et al. The global landscape of approved antibody therapies. Antib Ther. 2022;5(4):233–57. doi:10.1093/abt/tbac021. PMID: 36213257.
4. Townsend S, Fennell BJ, Apgar JR, Lambert M, McDonnell B, Grant J, Wade J, Franklin E, Foy N, Ni Shuilleabhain D, et al. Augmented binary substitution: single-pass CDR germ-lining and stabilization of therapeutic antibodies. Proc Natl Acad Sci U S A. 2015;112(50):15354–59. doi:10.1073/pnas.1510944112. PMID: 26621728.
5. Li B, Tesar D, Boswell CA, Cahaya HS, Wong A, Zhang J, Meng YG, Eigenbrot C, Pantua H, Diao J, et al. Framework selection can influence pharmacokinetics of a humanized therapeutic antibody through differences in molecule charge. MAbs. 2014;6(5):1255–64. doi:10.4161/mabs.29809. PMID: 25517310.
6. Ewert S, Honegger A, Pluckthun A. Stability improvement of antibodies for extracellular and intracellular applications: cDR grafting to stable frameworks and structure-based framework engineering. Methods. 2004;34(2):184–99. PMID: 15312672. doi:10.1016/j.ymeth.2004.04.007.
7. Kugler M, Stein C, Schwenkert M, Saul D, Vockentanz L, Huber T, Wetzel SK, Scholz O, Pluckthun A, Honegger A, et al. Stabilization and humanization of a single-chain Fv antibody fragment specific for human lymphocyte antigen CD19 by designed point mutations and CDR-grafting onto a human framework. Protein Eng Des Sel. 2009;22:135–47. doi:10.1093/protein/gzn079. PMID: 19188138.
8. Finlay WJ, Cunningham O, Lambert MA, Darmanin-Sheehan A, Liu X, Fennell BJ, Mahon CM, Cummins E, Wade JM, O'Sullivan CM, et al. Affinity maturation of a humanized rat antibody for anti-RAGE therapy: comprehensive mutagenesis reveals a high level of mutational plasticity both inside and outside the complementarity-determining regions. J Mol Biol. 2009;388:541–58. doi:10.1016/j.jmb.2009.03.019. PMID: 19285987.
9. Yu YJ, Watts RJ. Developing therapeutic antibodies for neurodegenerative disease. Neurotherapeutics. 2013;10(3):459–72. PMID: 23549647. doi:10.1007/s13311-013-0187-4.
10. Tang Y, Cao Y. Modeling pharmacokinetics and pharmacodynamics of therapeutic antibodies: progress, challenges, and future directions. Pharmaceutics. 2021;13(3):422. PMID: 33800976. doi:10.3390/pharmaceutics13030422.
11. Roopenian DC, Akilesh S. FcRn: the neonatal Fc receptor comes of age. Nat Rev Immunol. 2007;7(9):715–25. PMID: 17703228. doi:10.1038/nri2155.
12. Dall'acqua WF, Kiener PA, Wu H. Properties of human IgG1s engineered for enhanced binding to the neonatal Fc receptor (FcRn). J Biol Chem. 2006;281:23514–24. doi:10.1074/jbc.M604292200. PMID: 16793771.
13. Zalevsky J, Chamberlain AK, Horton HM, Karki S, Leung IW, Sproule TJ, Lazar GA, Roopenian DC, Desjarlais JR. Enhanced antibody half-life improves in vivo activity. Nat Biotechnol. 2010;28(2):157–59. PMID: 20081867. doi:10.1038/nbt.1601.
14. Roopenian DC, Christianson GJ, Sproule TJ. Human FcRn transgenic mice for pharmacokinetic evaluation of therapeutic antibodies. Methods Mol Biol. 2010;602:93–104. doi:10.1007/978-1-60761-058-8_6. PMID: 20012394.
15. Avery LB, Wang M, Kavosi MS, Joyce A, Kurz JC, Fan YY, Dowty ME, Zhang M, Zhang Y, Cheng A, et al. Utility of a human FcRn transgenic mouse model in drug discovery for early assessment and prediction of human pharmacokinetics of monoclonal antibodies. MAbs. 2016;8(6):1064–78. doi:10.1080/19420862.2016.1193660. PMID: 27232760.
16. Dobson CL, Devine PWA, Phillips JJ, Higazi DR, Lloyd C, Popovic B, Arnold J, Buchanan A, Lewis A, Goodman J, et al. Engineering the surface properties of a human monoclonal antibody prevents self-association and rapid clearance in vivo. Sci Rep. 2016; (1):6. doi:10.1038/srep38644.
17. Leipold D, Prabhu S. Pharmacokinetic and pharmacodynamic considerations in the design of therapeutic antibodies. Clin Transl Sci. 2019;12(2):130–39. PMID: 30414357. doi:10.1111/cts.12597.
18. Schoch A, Kettenberger H, Mundigl O, Winter G, Engert J, Heinrich J, Emrich T. Charge-mediated influence of the antibody variable domain on FcRn-dependent pharmacokinetics. Proc Natl Acad Sci U S A. 2015;112:5997–6002. doi:10.1073/pnas.1408766112. PMID: 25918417.
19. Datta-Mannan A, Thangaraju A, Leung D, Tang Y, Witcher DR, Lu J, Wroblewski VJ. Balancing charge in the complementarity-determining regions of humanized mAbs without affecting pI reduces non-specific binding and improves the pharmacokinetics. MAbs. 2015;7(3):483–93. PMID: 25695748. doi:10.1080/19420862.2015.1016696.
20. Hotzel I, Theil FP, Bernstein LJ, Prabhu S, Deng R, Quintana L, Lutman J, Sibia R, Chan P, Bumbaca D, et al. A strategy for risk mitigation of antibodies with fast clearance. MAbs. 2012;4(6):753–60. doi:10.4161/mabs.22189. PMID: 23778268.
21. Dostalek M, Prueksaritanont T, Kelley RF. Pharmacokinetic de-risking tools for selection of monoclonal antibody lead

candidates. MAbs. 2017;9(5):756–66. PMID: 28463063. doi:10.1080/19420862.2017.1323160.
22. Kelly RL, Sun T, Jain T, Caffry I, Yu Y, Cao Y, Lynaugh H, Brown M, Vasquez M, Wittrup KD, et al. High throughput cross-interaction measures for human IgG1 antibodies correlate with clearance rates in mice. MAbs. 2015;7(4):770–77. doi:10.1080/19420862.2015.1043503. PMID: 26047159.
23. Sharma VK, Patapoff TW, Kabakoff B, Pai S, Hilario E, Zhang B, Li C, Borisov O, Kelley RF, Chorny I, et al. In silico selection of therapeutic antibodies for development: viscosity, clearance, and chemical stability. Proc Natl Acad Sci U S A. 2014;111:18601–06. doi:10.1073/pnas.1421779112. PMID: 25512516.
24. Avery LB, Wade J, Wang M, Tam A, King A, Piche-Nicholas N, Kavosi MS, Penn S, Cirelli D, Kurz JC, et al. Establishing in vitro in vivo correlations to screen monoclonal antibodies for physicochemical properties related to favorable human pharmacokinetics. MAbs. 2018;10(2):244–55. doi:10.1080/19420862.2017.1417718. PMID: 29271699.
25. Afroz T, Chevalier E, Audrain M, Dumayne C, Ziehm T, Moser R, Egesipe AL, Mottier L, Ratnam M, Neumann M, et al. Immunotherapy targeting the C-terminal domain of TDP-43 decreases neuropathology and confers neuroprotection in mouse models of ALS/FTD. Neurobiol Dis. 2023;179:106050. doi:10.1016/j.nbd.2023.106050. PMID: 36809847.
26. Ling SC, Polymenidou M, Cleveland DW. Converging mechanisms in ALS and FTD: disrupted RNA and protein homeostasis. Neuron. 2013;79(3):416–38. PMID: 23931993. doi:10.1016/j.neuron.2013.07.033.
27. Afroz T, Hock EM, Ernst P, Foglieni C, Jambeau M, Gilhespy LAB, Laferriere F, Maniecka Z, Pluckthun A, Mittl P, et al. Functional and dynamic polymerization of the ALS-linked protein TDP-43 antagonizes its pathologic aggregation. Nat Commun. 2017;8(1):45. doi:10.1038/s41467-017-00062-0. PMID: 28663553.
28. Lukavsky PJ, Daujotyte D, Tollervey JR, Ule J, Stuani C, Buratti E, Baralle FE, Damberger FF, Allain FH. Molecular basis of UG-rich RNA recognition by the human splicing factor TDP-43. Nature Structural & Molecular Biology. 2013;20(12):1443–49. PMID: 24240615. doi:10.1038/nsmb.2698.
29. Ayala YM, Zago P, D'Ambrogio A, Xu YF, Petrucelli L, Buratti E, Baralle FE. Structural determinants of the cellular localization and shuttling of TDP-43. J Cell Sci. 2008;121:3778–85. doi:10.1242/jcs.038950. PMID: 18957508.
30. Neumann M, Sampathu DM, Kwong LK, Truax AC, Micsenyi MC, Chou TT, Bruce J, Schuck T, Grossman M, Clark CM, et al. Ubiquitinated TDP-43 in frontotemporal lobar degeneration and amyotrophic lateral sclerosis. Science. 2006;314(5796):130–33. doi:10.1126/science.1134108. PMID: 17023659.
31. Polymenidou M, Cleveland DW. The seeds of neurodegeneration: prion-like spreading in ALS. Cell. 2011;147(3):498–508. PMID: 22036560. doi:10.1016/j.cell.2011.10.011.
32. Porta S, Xu Y, Restrepo CR, Kwong LK, Zhang B, Brown HJ, Lee EB, Trojanowski JQ, Lee VM. Patient-derived frontotemporal lobar degeneration brain extracts induce formation and spreading of TDP-43 pathology in vivo. Nat Commun. 2018;9(1):4220. PMID: 30310141. doi:10.1038/s41467-018-06548-9.
33. Kawakami I, Arai T, Hasegawa M. The basis of clinicopathological heterogeneity in TDP-43 proteinopathy. Acta Neuropathol. 2019;138(5):751–70. PMID: 31555895. doi:10.1007/s00401-019-02077-x.
34. Betts A, Keunecke A, van Steeg TJ, van der Graaf PH, Avery LB, Jones H, Berkhout J, van Steeg TJ, van der Graaf PH. Linear pharmacokinetic parameters for monoclonal antibodies are similar within a species and across different pharmacological targets: a comparison between human, cynomolgus monkey and hFcRn Tg32 transgenic mouse using a population-modeling approach. MAbs. 2018;10(5):751–64. PMID: 29634430. doi:10.1080/19420862.2018.1462429.
35. Kasai T, Kojima Y, Ohmichi T, Tatebe H, Tsuji Y, Noto YI, Kitani-Morii F, Shinomoto M, Allsop D, Mizuno T, et al. Combined use of CSF NfL and CSF TDP-43 improves diagnostic performance in ALS. Ann Clin Transl Neurol. 2019;6(12):2489–502. doi:10.1002/acn3.50943. PMID: 31742901.
36. Liu S, Verma A, Kettenberger H, Richter WF, Shah DK. Effect of variable domain charge on in vitro and in vivo disposition of monoclonal antibodies. MAbs. 2021;13(1):1993769. PMID: 34711143. doi:10.1080/19420862.2021.1993769.
37. Tabrizi M, Bornstein GG, Suria H. Biodistribution mechanisms of therapeutic monoclonal antibodies in health and disease. Aaps J. 2010;12(1):33–43. PMID: 19924542. doi:10.1208/s12248-009-9157-5.
38. Igawa T, Tsunoda H, Tachibana T, Maeda A, Mimoto F, Moriyama C, Nanami M, Sekimori Y, Nabuchi Y, Aso Y, et al. Reduced elimination of IgG antibodies by engineering the variable region. Protein Eng Des Sel. 2010;23:385–92. doi:10.1093/protein/gzq009. PMID: 20159773.
39. Bumbaca Yadav D, Sharma VK, Boswell CA, Hotzel I, Tesar D, Shang Y, Ying Y, Fischer SK, Grogan JL, Chiang EY, et al. Evaluating the use of antibody variable region (Fv) Charge as a risk assessment tool for predicting typical cynomolgus monkey pharmacokinetics. J Biol Chem. 2015;290:29732–41. doi:10.1074/jbc.M115.692434. PMID: 26491012.
40. Ober RJ, Radu CG, Ghetie V, Ward ES. Differences in promiscuity for antibody–FcRn interactions across species: implications for therapeutic antibodies. Int Immunol. 2001;13(12):1551–59. PMID: 11717196. doi:10.1093/intimm/13.12.1551.
41. Andersen JT, Daba MB, Berntzen G, Michaelsen TE, Sandlie I. Cross-species binding analyses of mouse and human neonatal Fc receptor show dramatic differences in immunoglobulin G and albumin binding. J Biol Chem. 2010;285:4826–36. doi:10.1074/jbc.M109.081828. PMID: 20018855.
42. Dunbar J, Krawczyk K, Leem J, Marks C, Nowak J, Regep C, Georges G, Kelm S, Popovic B, Deane CM. SAbPred: a structure-based antibody prediction server. Nucleic Acids Res. 2016;44(W1):W474–478. PMID: 27131379. doi:10.1093/nar/gkw361.
43. Eisenberg D, Schwarz E, Komaromy M, Wall R. Analysis of membrane and surface protein sequences with the hydrophobic moment plot. J Mol Biol. 1984;179:125–42. doi:10.1016/0022-2836(84)90309-7. PMID: 6502707.
44. Kozlowski LP. IPC 2.0: prediction of isoelectric point and pKa dissociation constants. Nucleic Acids Res. 2021;49:W285–W92. doi:10.1093/nar/gkab295. PMID: 33905510.
45. Almagro JC, Fransson J. Humanization of antibodies. FBL. 2008;13:1619–33. doi:10.2741/2786.
46. Jain T, Sun T, Durand S, Hall A, Houston NR, Nett JH, Sharkey B, Bobrowicz B, Caffry I, Yu Y, et al. Biophysical properties of the clinical-stage antibody landscape. Proc Natl Acad Sci U S A. 2017;114:944–49. doi:10.1073/pnas.1616408114. PMID: 28096333.